Taylor & Francis
Taylor & Francis Group

Automatika

Journal for Control, Measurement, Electronics, Computing and Communications

ISSN: 0005-1144 (Print) 1848-3380 (Online) Journal homepage: https://www.tandfonline.com/loi/taut20

Performance evaluation of a portable 3D vision coordinate measuring system

Octavio Icasio-Hernández, José-Joel González-Barbosa, Yajaira-Ilse Curiel-Razo & Juan B. Hurtado-Ramos

To cite this article: Octavio Icasio-Hernández, José-Joel González-Barbosa, Yajaira-Ilse Curiel-Razo & Juan B. Hurtado-Ramos (2017) Performance evaluation of a portable 3D vision coordinate measuring system, Automatika, 58:3, 253-265, DOI: 10.1080/00051144.2017.1391616

To link to this article: https://doi.org/10.1080/00051144.2017.1391616

Published online: 09 Feb 2018.

AUTOMATIKA, 2017
VOL. 58, NO. 3, 253–265
https://doi.org/10.1080/00051144.2017.1391616

Taylor & Francis
Taylor & Francis Group

REGULAR PAPER

OPEN ACCESS Check for updates

Performance evaluation of a portable 3D vision coordinate measuring system

Octavio Icasio-Hernández[a,b], José-Joel González-Barbosa[b], Yajaira-Ilse Curiel-Razo[b] and Juan B. Hurtado-Ramos[b]

[a]Centro Nacional de Metrología, CENAM, el Marqués, Mexico; [b]Instituto Politécnico Nacional, CICATA Querétaro, Col Colinas del Cimatario, Mexico

ABSTRACT

In this work, we present a portable 3D vision coordinate measuring machine (PCMM) for short range-real time photogrammetry. The PCMM performs 3D measurements of points using a single camera in combination with a hand tool and a computer. The hand tool has infrared LEDs serving as photogrammetric targets. The positions of these targets were pre-calibrated with an optical coordinate-measuring machine defining a local coordinate system on the hand tool. The camera has an infrared filter to exclude all ambient light but infrared targets. Positions of the imaged infrared targets are converted to 3D coordinates using pixel positions and pre-calibrated positions of the targets. Also, we present a set of criteria for selecting the infrared LEDs and the camera filter, a camera calibration method, a tracking and POSE algorithms, and a 3D coordinate error correction for the PCMM. The correction is performed using the PCMM as a range meter, which implies comparing the 3D coordinate points of the PCMM with a coordinate measuring machine, and then generating a look up table (LUT) for correction. The global error of the PCMM was evaluated under ASME B89.4.22-2004. Sphere and single point errors were around 1 mm, volumetric error were under 3 mm.

ARTICLE HISTORY
Received 17 August 2017
Accepted 4 October 2017

KEYWORDS
Photogrammetry; LUT; portable CMM 'sphere test; single point test; volumetric test

1. Introduction

Opto-mechanical devices for dimensional and geometrical measurements have been present since close range photogrammetry in industry became technically and economically successful in the mid-1980s (see [1]). The portable 3D vision coordinate measuring machine (PCMM) is a perfect mechanical contact complement to a touchless optical measuring device, since it can measure objects that a touchless device cannot reach, such as inner holes. Also, because of its important applications, especially in the automotive and aircraft industries, the PCMM must be as accurate as possible. In fact, the PCMM is broadly employed for measuring large constructions, hidden points and crash vehicles, among others. To measure PCMM accuracy, the performance evaluation must be conducted based on specific standards, which is part of the goal of this paper.

Luhmann [1] and Hocken et al. [2] proposed examples of opto-mechanical devices, such articulated arms coordinated measuring machines (AACMM), laser trackers, photogrammetric systems and PCMM. In this work, we designed a PCMM using a camera, a hand tool with a spherical probe tip and optical targets on it, and a laptop computer (see Figure 1). PCMM devices record trough the camera, the computer and the optical targets, the 3D position of the spherical probe tip touching the object surface at points of interest. References [2–7] report some designed PCMM. Commercial examples include SOLO system, by Metronor company, ATOS (including a hand tool accessory), by GOM, MI probe, developed by Creaform, and T-Point CS, by Steinbichler among others (see [1]). The way these commercial PCMMs work is similar to how our own PCMM functions; however, their software and hardware components are not of public domain.

Our idea of designing and building a PCMM arose after consulting Hocken et al. [2], Liu et al. [3] and Amdal [4]. As for the building process, we noticed that Hocken's mathematical model to get 3D coordinates was not accurate enough (results from using this model are discussed in Section 6 and Figure 7). Also, we noticed that Liu et al. [3] presented the same mathematical model. They reported average errors in Z direction under 0.26 mm with 450 mm depth travel when using the PCMM as a range meter, and after 50 samples in average with almost 4 mm of dispersion. On the other hand, Amdal [4] described a general mathematical model for perspective transformations and demonstrated the repeatability of his PCMM measuring only one point at different distances. Amdal's results showed single point measurement errors below 0.2 mm, yet the calibration method is not described.

Liu et al. [5] discussed the mathematical model for calibrating the spherical probe tip center position of a

CONTACT Octavio Icasio-Hernández oicasio@cenam.mx

PCMM. Our work is very similar to Liu et al.'s [5] as regards the number of targets; however, the probe tip of our PCMM is calibrated together with its targets, which impedes its change, unless a new calibration is performed. Moreover, Li et al. [6] proposed a PCMM using two cameras, since measurement errors reported in their work and in Xiao et al. [7] suggested that two or more cameras increased accuracy of a PCMM. Our work demonstrates that with a simple Look up Table (LUT), measurement errors decrease using only one camera.

To develop our PCMM, we took as basis suggestions from [2–7] to design the hand tool, whereas we consulted Lepetit et al. [8]'s mathematical model to get the position and orientation (POSE) of the hand tool with respect to the camera coordinate system. Other computer vision methods for getting the POSE are proposed in [9–16], yet these methods were excluded because the iteration process of their algorithms was time consuming. As regards the camera calibration, we relied on Zhang's technique [17], implemented by Bouguet's toolbox [18], yet additional and equally useful calibration methods are reported in [19–23].

The aim of this work is to propose a methodology to get a PCMM prototype for measuring 3D coordinates. Additionally, we describe a method for correcting these 3D coordinates using a coordinate measuring machine (CMM) and a LUT. The correction allows for measurement errors below 1.2 mm when the hand tool is used as a range meter, which implies moving it without rotations toward or away from the camera (Z direction), and below 0.5 mm when the hand tool is maintained at a certain distance away from the camera, thus avoiding rotations. We evaluated the global measurement errors of the PCMM using ASME B89.4.22-2004 standard (see [24]), considering the PCMM as an AACMM.

The remainder of this paper is organized as follows. Section 2 introduces our proposed PCMM, Section 3 discusses the camera calibration method and Section 4 describes the tracking and POSE algorithm, which are the core of the PCMM. Then, Section 5 reports results from using the PCMM as a range meter and its performance evaluation, using ASME B89.4.22-2004 standard. Finally, Section 6 presents our conclusions.

2. Proposed PCMM

Figure 1 depicts the proposed PCMM. It consists of a specially designed hand tool, made of carbon fiber and aluminium, with a spherical probe tip and infrared LEDs on it, one CMOS camera and a laptop computer. The carbon fiber has a coefficient of thermal expansion close to zero, which avoids expansion and contraction of the hand tool, thus reducing dimensional errors caused by temperature. Similarly, there are 10 infrared LEDs on the hand tool, a touch trigger spherical probe tip and a button. The button activates a Bluetooth module sending a wireless signal to the computer to record the point where the probe tip is making contact. The 10 infrared light sources and the probe tip must be referenced to a local hand tool coordinate system.

During measurements, the spherical probe tip touches the object's surface to be measured, and an image from the infrared light sources on the hand tool is captured with the camera and processed by a POSE algorithm in the computer (see Figure 5(c)). As a result, a 3D coordinate of the contact point on the object's surface is calculated. Section 4 explains in detail how to obtain the 3D coordinate point. Geometrical features of objects, such as dimensions, form, and position errors among others can be evaluated with software handling 3D point coordinates provided by

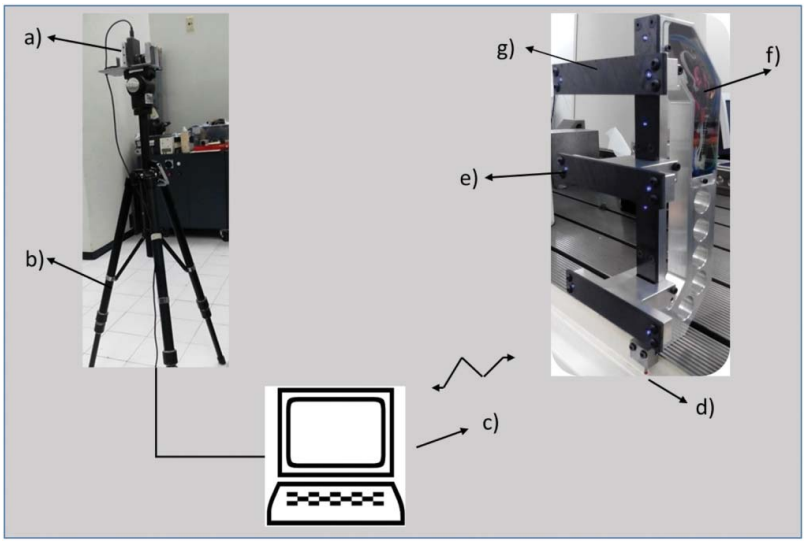

Figure 1. Proposed PCMM. (a) CMOS camera, (b) tripod, (c) computer, (d) spherical probe tip, (e) infrared LEDs, (f) Bluetooth module (g) and carbon fiber structure.

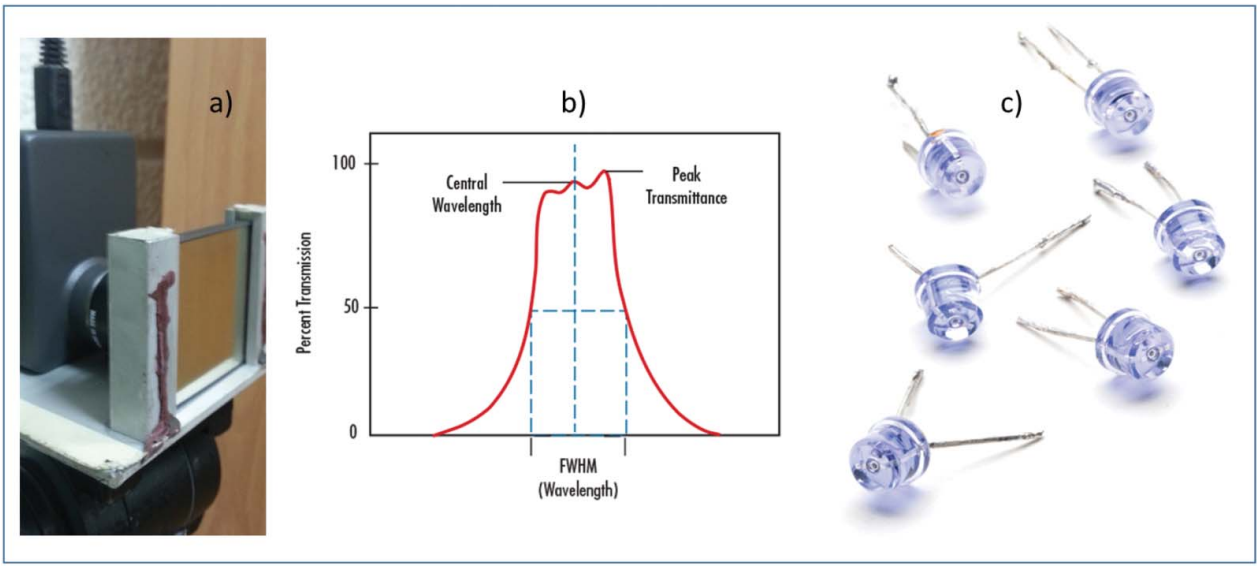

Figure 2. (a) Camera and infrared band pass filter with CWL = 950 nm and FWHM = 8 nm. (b) Illustration of center wavelength and full width at half maximum. (c) Infrared commercial LEDs.

the PCMM, such as CMM measuring software. In this sense, the proposed PCMM is only a tool to collect 3D coordinate points.

2.1. Infrared filter and LEDs selection

The camera is characterized by a monochromatic CMOS sensor, 1280 (H) by 1024 (V) resolution, pixel pitch of 5.2 μm by 5.2 μm, and a focal lens length equal to 3.6 mm. The infrared-passing band pass filter, which is set in front of the camera, has a center wavelength (CWL) of 950 nm and a bandwidth or full width at half maximum (FWHM) of 8 nm (see Figure 2(a,b)). We selected the CWL after all infrared LEDs were measured with a spectrometer, and every LED was determined to emit around that CWL value. Figure 6 shows the CWL and FWHM of one of the LEDs. The filter's CWL and FWHM avoid light noise from other sources.

The infrared LEDs were cut by a cross-section to obtain a better definition of circles on the CMOS image plane. The original shape of LEDs produced a geometry that is unlike a circle, yet it is important to project circles on the image plane because its position is calibrated using the circle centroid. Although some commercial LEDs already emit circle-shaped light (round LED light), they were not available for us at the time of the tests. Figure 2(c) show these LEDs.

As in Liu et al. [5], we selected 10 LEDS. Taking into account our results (see Section 5.3) and those obtained by Liu et al. [3], with errors over 1 mm, we concluded that the LEDs positions on our hand tool were not collinear, but in a plane orientation. This phenomenon could have been caused by the way the LEDs were arranged, and it avoided hand tool orientation errors (see Liu et al. [3]).

Also, in this work we used infrared LEDs that required a source of energy to power them. Instead of these LEDs, it is possible to use retroreflector targets on the hand tool. The targets would help remove the filter set in front of the camera and take off the source of energy, yet with them the tracking algorithm would be affected by ambient light and background noise.

3. Camera calibration

The camera calibration of our PCMM was based on Bouguet's toolbox (see [18]). Figure 3 shows the images used for the calibration. We employed a checkerboard calibration pattern made of soda-lime glass with chrome coating. The squares' width and height was 4 mm, with an uncertainty of 3.7 μm. Also, we recommend that the calibration pattern images cover the space where the measurements of interest will be made with the PCMM. Similarly, the checkerboard must have different POSEs preferably, close and away from the camera.

Our camera calibration method was also based on the pinhole model, often called collinear model (see [19]). Figure 4 shows the pinhole model taking into account the PCMM. The calibration consisted in finding the camera's intrinsic (K matrix) and extrinsic parameters $(R_p,\ T_p)$. Intrinsic parameters allowed us to change from the camera coordinate system to the image plane or vice versa (The K matrix has information on focal length (fc), scalar factor(s), a radial and tangential coefficient to represent lens distortions (kc) and a 2D pixel image center (cc)). Extrinsic parameters represent the object's POSE in the real world referred to the camera coordinate system. The camera coordinate system has its origin

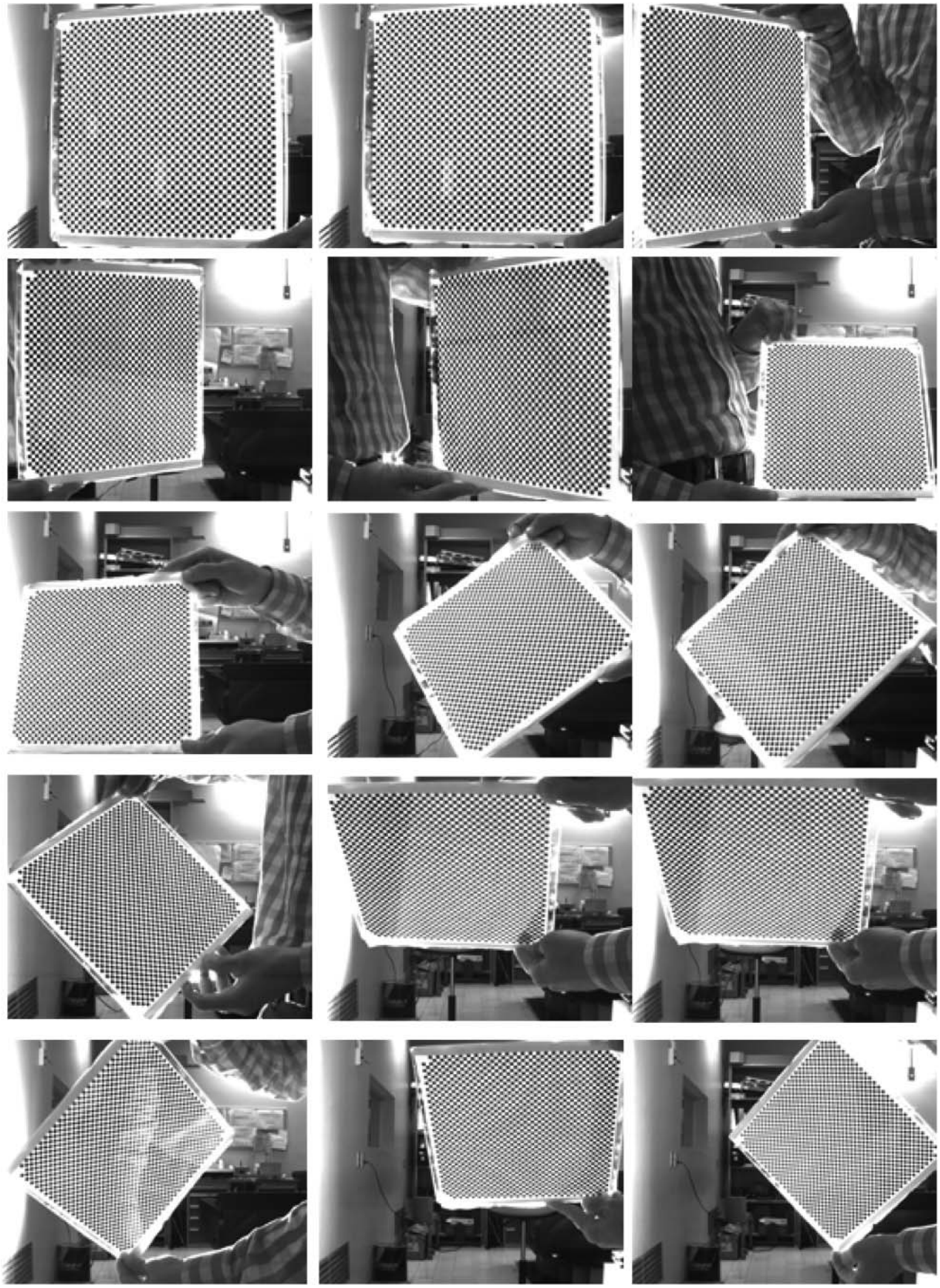

Figure 3. Sequence of images used for camera calibration.

at the point where the optical rays coming from the lens cross the optical axis, the X_c, Y_c camera axis are parallel to the u, v axis of the image plane (see Figure 4).

Intrinsic parameters do not change unless the camera's focal length changes. In a PCMM, the camera POSE and focal length should be fixed. In the results section, we present the intrinsic parameters to convert

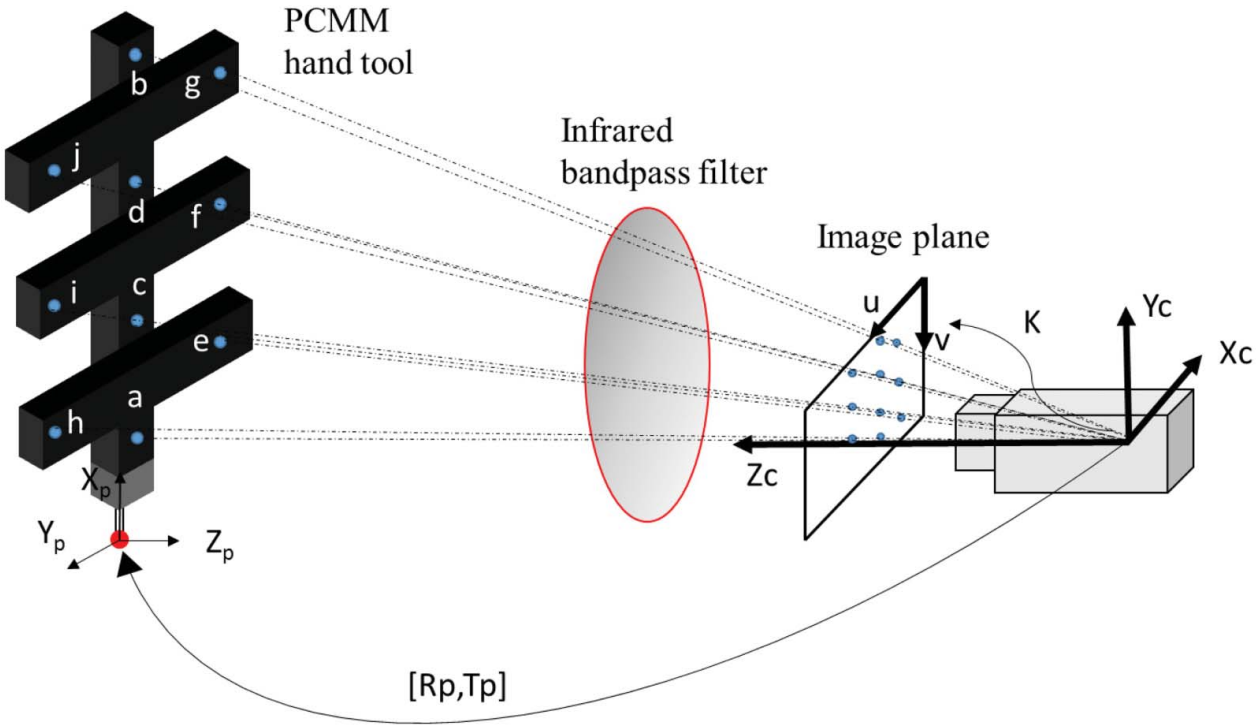

Figure 4. Schematic showing the definition of PCMM components' coordinates system when using the pinhole model for the camera.

pixels to units of length. On the other hand, extrinsic parameters or POSE of each checkerboard image from Figure 3, calculated using Bouguet's toolbox, could be used as a reference coordinate system, yet in our case, the hand tool's POSE $(R_p,\ T_p)$ is referenced to the camera coordinate system $X_c,\ Y_c, Z_c$, as shown in Figure 4.

4. Tracking and pose algorithm

Figure 5(b) shows 10 infrared LEDs (a- $-$ j) to be tracked and ordered and Figure 5(c) shows those 10 LEDs already tracked and ordered with Algorithm 1. Because the hand tool can adopt any POSE during the objects' measurement, the tracking algorithm and each LED order will both define how the hand tool's POSE and the 3D coordinate point of the spherical probe tip are obtained. The Algorithm 1 is a Matlab script and uses the regionprops function to track the subpixel centroid of each infrared LED. Note that with the infrared filter set in front of the camera, only the light emitted by the infrared LEDs passes, so the image contains 10 or less "speckles" produced by the LEDs (see Figure 5(c)).

As mentioned in Section 1, we calculated the hand tool's POSE with respect to the camera coordinate system using Lepetit et al.'s [8] algorithm. This algorithm needs three parameters as input: at least four 3D calibrated world points and its corresponding four 2D pixel positions, and the intrinsic camera parameters. The algorithm then calculates the rotation and translation of the camera coordinate system on world reference and the infrared LEDs' position in the camera coordinate system. As mentioned before, each 3D calibrate world point from the hand tool must have its corresponding 2D pixel point. To achieve this, Algorithm 1 calculates 10 2D ordered pixel positions of each infrared LED on the hand tool. Figure 5(a) shows the optical coordinate measuring machine (OCMM) used to get the 10 calibrated 3D points of each infrared LED with respect to the spherical probe tip. On the other hand, Figure 5(b) shows the local coordinate system used during the calibration. The Z primary axis is defined with the least square fitted plane using e–j centroid LEDs, the X secondary axis is defined with a least square fitted line passing through the centroid of the spherical probe tip and centroid of b LED, Y-axis is perpendicular to X-, Z-axis and the origin is on the centroid of the spherical probe tip. Once the local coordinate system was defined, the infrared LEDs and the spherical probe tip were measured by computing centroids. Our PCMM can use only probe tips of the same length, because it is part of the calibration; however, if a dynamic probe tip change is desired, Liu et al.'s calibration method can be employed [5].

5. Experimental results

5.1. Center wavelength of an infrared commercial LED

Figure 6 shows the CWL of one of the most popular and cheap infrared LEDs. The wavelength of the light

Algorithm 1: LEDs tracking and ordering

```
function [Cn] = track_order(I)
%binary image
L = logical(~(I < 255));
%Start LEDs tracking
s = regionprops(L,'PixelIdxList','PixelList');
%Compute subpixel intensity-weighted centroids
for k = 1 : numel(s)
 idx = s(k).PixelIdxList;
 pv = double(I(idx));
 sumpv = sum(pv);
 x = s(k).PixelList(:, 1);
 y = s(k).PixelList(:, 2);
 xb = sum(x.* pv) / sumpv;
 yb = sum(y. *pv) / sumpv;
 C = [C; xb yb];
 end
%Start ordering centroids by computing a general centroid, cen
cen = [mean(C(1, :)); mean(C(2, :))];
%calculate distance of each centroid to cen and order centroids
%in descending order using indexes calculated with distances
dr = sqrt((cen(1) − C(1, 1 : length(C))).^2 + (cen(2) − C(2, 1 : length(C))).^2);
 [dr_a, ia] = sort(dr,'descend');
 Ca = C(:, ia);
 %Accumulated distances between a point and the rest of the points
 da = sqrt((Ca(1, 1 : length(C)) − Ca(1, 1)).^2 + (Ca(2, 1 : length(C)) − Ca(2, 1)).^2);
%the next code ensures that a LED is the first point of vector Ca
[~, ipb] = max(da);
 if ipb~ = 2
 aux = Ca(:, 2);
 Ca(:, 2) = Ca(:, ipb);
 Ca(:, ipb) = aux;
 end
%Evaluate a straight line between the first two elements of C (Points a, b of
%Figure 5(b)). This gives us slope m and intersect b. Then, determine which points
%are to the right or left of the straight line around 5 pixels that must be
%enclosed to the line. There is an additional code (not here) to know whether
%the points are over or under the straight line.
m = (Ca(2, 1) − Ca(2, 2))/((Ca(1, 1) − Ca(1, 2)));
 b = Ca(2, 1) − (m*Ca(1, 1));
 mult = 1;
 if m < 0 : mult = -1;
 for i = 3 to length (C)
 yp = m*Ca(1, i) + b;
 s = (yp − Ca(2, i))*mult;
 if s≥ − 5 and s≤5 ind1 = [ind1 i]; %save index points c–d
If s > 5 : ind2 = [ind2 i]; %save index points e–g
If s < − 5 : ind3 = [ind3 i] ; %save index points h–j
end
%Discriminate between points c–d, e–g, h–j
%order each index in ascending order with accumulated distances
[cd, ir] = sort(da(ind1));
 [efg, ier] = sort(da(ind2));
 [hij, idr] = sort(da(ind3));
 %from points on the straight line save c and d
 iro = ind1(ir);
 %from points to the right of the straight line save, e,f,g
 iero = ind2(ier);
 %from points to the left of the straight line save, h,i,j
 idro = ind3(idr);
 %Reorder original centroids
 Cn = Ca;
 if length(iro) = = 2 && length(iero) = = 3 && length(idro) = = 3
 Cn(:, 3 : 4) = Ca(:, iro);
 Cn(:, 5 : 7) = Ca(:, iero);
 Cn(:, 8 : 10) = Ca(:, idro);
 end
```

emitted by the infrared LED was measured using a Thorlab's spectrometer. The peak value is approximately on 948 nm, which is enclosed by the 8-nm bandwidth of the 950-nm infrared band pass filter set in front of the camera. The selection of the filter depends on the LEDs' wavelength. Figure 6 allowed us to select the infrared band pass filter.

5.2. Camera calibration

Table 1 shows the intrinsic parameters using images from Figure 3 as input parameters for Bouguet's toolbox [18].

The quality of the calibration depends on the uncertainty of the parameters. The lower the uncertainty

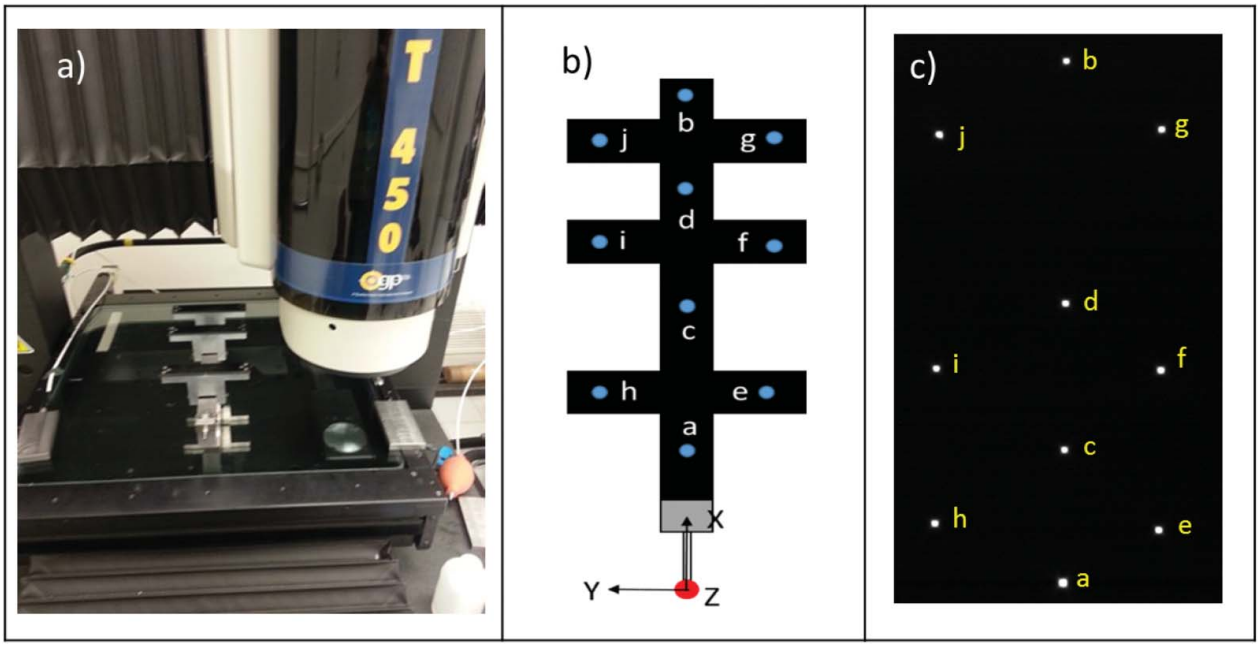

Figure 5. (a) OCMM calibrating each LED and spherical probe tip position of the hand tool. (b) Local coordinate system of the hand tool with labelled infrared LEDs. (c) Image of infrared LEDs viewed by the camera and tracked-ordered with Algorithm 1.

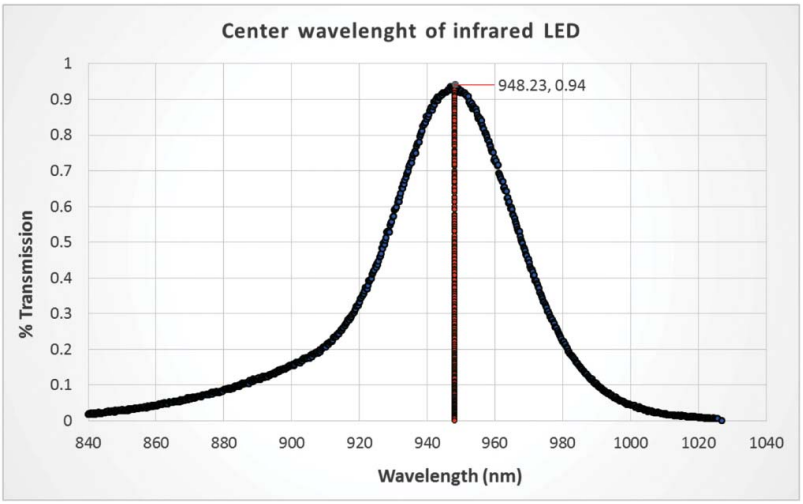

Figure 6. Center wavelength of a commercial infrared LED.

reported by the toolbox, the better the calibration. According to Zhu et al. [23], who performed an uncertainty and sensitivity analysis in camera calibration, the principal point of intrinsic parameters (see *cc* on Table 1) is one from the parameters which highly influences the conversion between pixel and units of length. This would be the case if the lens's distortion was significant, since the lens's distortion correction depends not just on distortion coefficients (see *kc* on Table 1), but on the principal point. In our case, we considered that the focal length (see *fc* on Table 1) has more influence on dimensional measurements with the PCMM, since this parameter represents a dimensional scale factor. Finally, according to Amdal [4], the main measurement errors come with the incorrect PCMM's POSE on the camera coordinate system. This is something to be explored to improve measurement accuracy.

Table 1. Intrinsic parameters from camera calibration using Bouguet [18].

Parameter	Value	Uncertainty
Focal length (*fc*)	[2317.7877; 2317.5668]	[0.8554; 0.8506]
Principal point (*cc*)	[653.1255; 516.8321]	[1.4581; 1.4173]
Skew coefficient (alpha_*c*)	0.0000	0.0000
Distortion coefficients (*kc*)	[−0.3812; 0.1908; 0.0014; −0.0005; 0.0000]	[0.0024; 0.0266; 0.0001; 0.0001; 0.0000]

5.3. Performance evaluation and correction of PCMM used as range meter

We started with a PCMM based on Hocken et al. [2] and Liu et al. [3], considering only three quasi collinear infrared LEDs (see Figure 7(a)). Figure 7(b) shows the results using the PCMM as range meter and using the

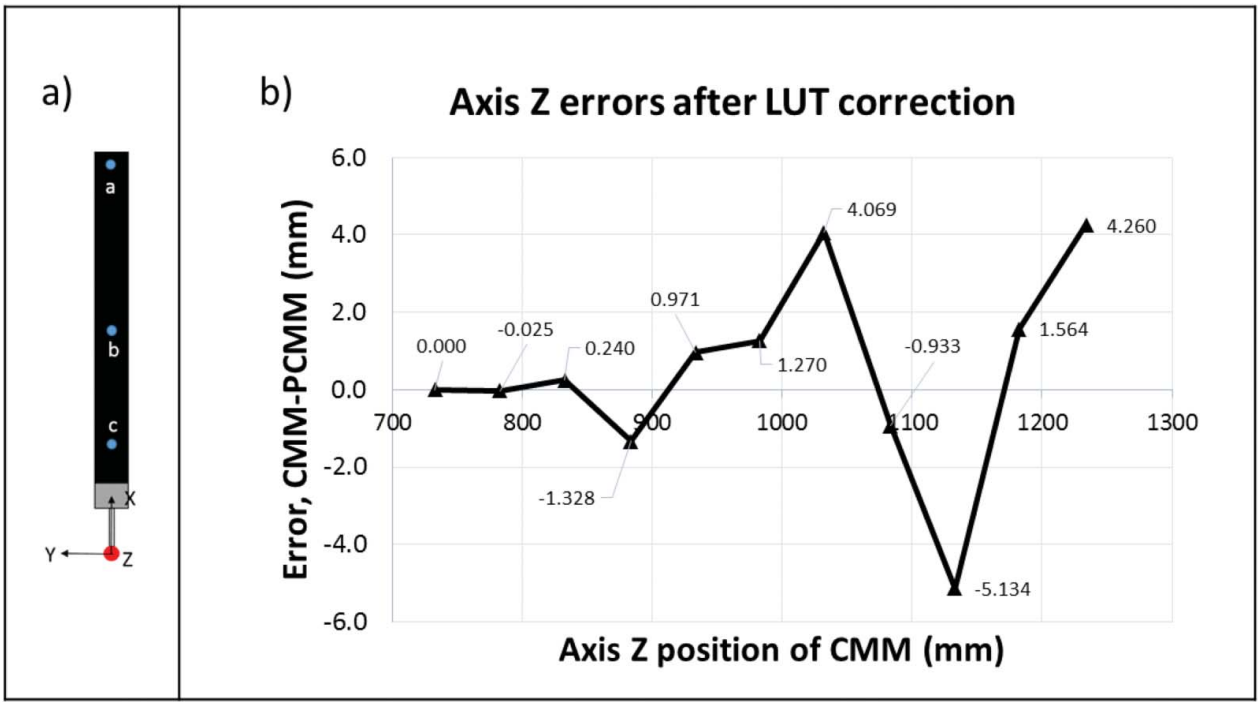

Figure 7. (a) First prototype of PCMM. (b) Results using the PCMM as range meter in *Z* direction close and far away from the camera after LUT correction.

average of three measurements. Range meter means to measure using only one axis of the PCMM, avoiding rotations and translations in the other axis. From Figure 7(b) to Figure 9, we can see range meter errors in *Z* direction, which is the axis with less accuracy, since it measures the distance between the camera and the hand tool.

The results obtained after correcting the PCMM with a LUT are shown in Figure 7(b). The LUT was evaluated following the next steps:

(1) Setup the PCMM as shown in Figure 8(a), where the PCMM is on the moving table of a CMM and its movement allows for the PCMM's *Z*-coordinate to increase or decrease.

(2) Align the PCMM's coordinate system $(X_{\text{pcmm}}, Y_{\text{pcmm}}, Z_{\text{pcmm}})$ against the CMM's coordinate system $(X_{\text{cmm}}, Y_{\text{cmm}}, Z_{\text{cmm}})$. This means that one axis of the CMM must be collinear with another axis of the PCMM. In our case, the PCMM's *Z*-axis was collinear with the CMM's *X*-axis (see Figure 8(a)). Follow the next steps to perform the alignment:

(a) Move the CMM until the PCMM is in its initial position as close to the camera as possible

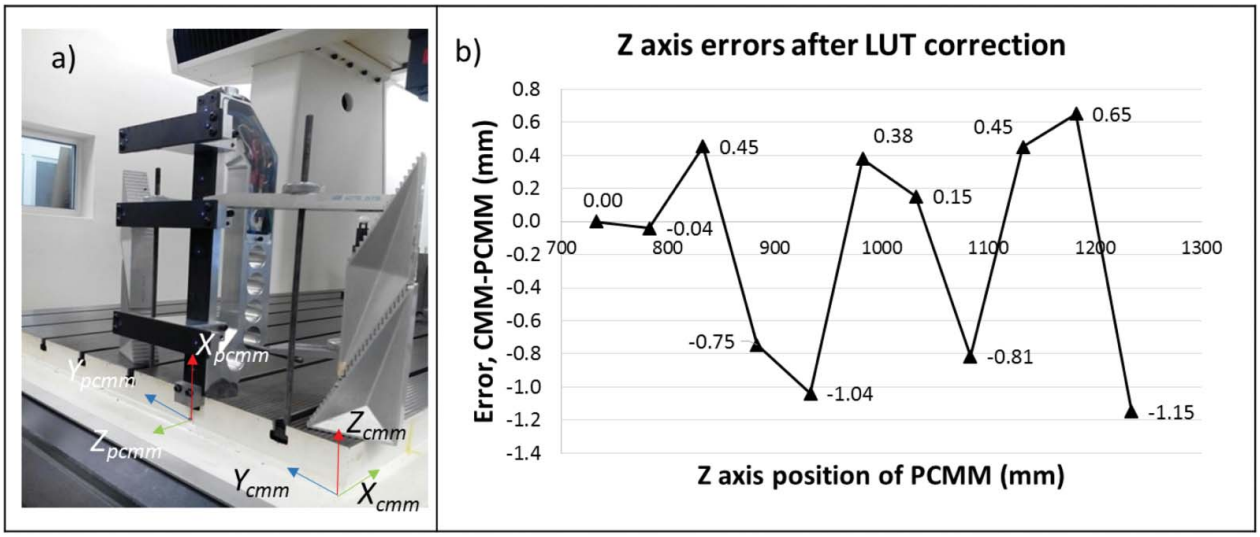

Figure 8. (a) Setup to use the PCMM as range meter. (b) Results of PCMM as range meter in *Z*-axis direction close and far away from camera after LUT correction.

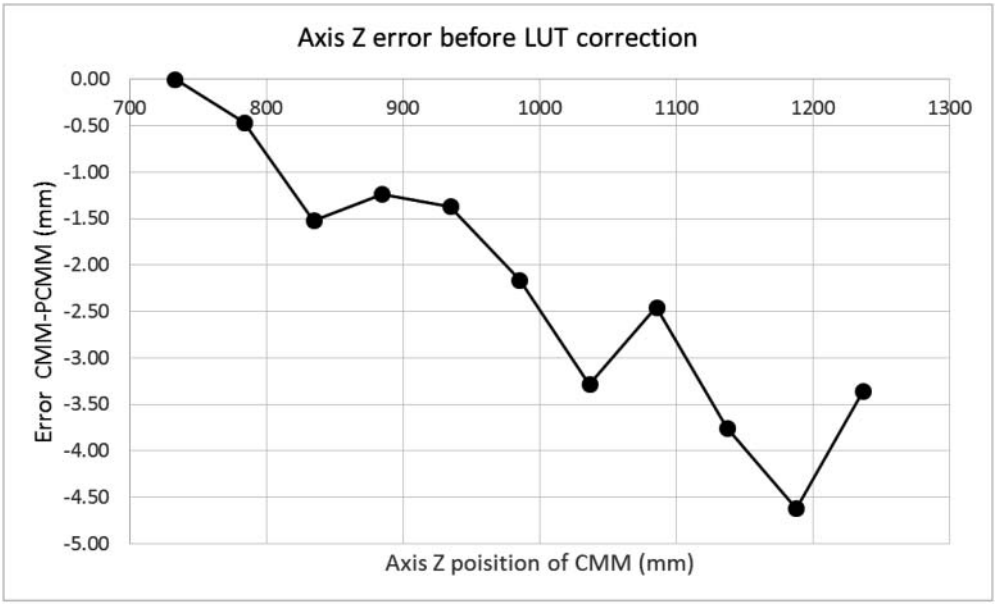

Figure 9. Results of PCMM as range meter in *Z*-axis direction close and far away from camera before LUT correction.

(it depends on the range where the 10 hand tool LEDs are in view to the camera).

(b) Make a translation of the camera until X_{pcmm} and Y_{pcmm} are close to zero.

(c) Move the CMM to the end position of the PCMM; this could be the range where the measurements will be performed or the CMM's scale interval.

(d) Rotate the camera until X_{pcmm} and Y_{pcmm} are close to zero.

(e) Repeat steps *a*–*d* until X_{pcmm} and Y_{pcmm} are close to zero during the whole CMM's run path.

Note: The camera must be set on a table or tripod for translations and rotations. With a CMM where the entire bridge moves instead of the table, it is recommended to rotate and translate the coordinate system of the CMM to that of the PCMM.

(3) Stop the CMM at different positions, which will represent the first column positions of the LUT (we recommend at least five interval positions where the PCMM will measure). In each stop position, evaluate PCMM errors (CMM position minus PCMM position). These errors will be the second column of the LUT.

(4) Repeat steps 1–3 for X and Y PCMM coordinates; this will give us a LUT for each coordinate.

(5) Finally, an interpolation function will receive as input parameters X, Y, Z LUTs and the current X, Y, Z position of the PCMM to perform the correction when the PCMM is measuring an object. If the current PCMM position is not exactly on a column position of the LUT, a linear interpolation is applied. If the current position of the PCMM is outside the LUT column positions, the first or last LUT error must be used for correction. In our case, we did not perform extrapolation; instead, we fixed the errors on the LUT's extremes.

Because of results presented in Figure 7(b), we referred to Liu et al. [5] to propose a different prototype using more infrared LEDs in different planes. Figure 8(a) shows the setup of this PCMM prototype set in a CMM machine. Figure 8(b) shows the results using the PCMM as range meter in Z direction and using the average of three measurements. The Z Z-axis of Figure 8(b) shows the distance measurement reported by the CMM scales, minus PCMM; the Z Z-axis shows how far away the hand tool was from the camera, covering from 750 to 1250 mm, approximately.

We added more LEDs on 3D positions to reduce PCMM orientation errors. In this sense, Figure 8(b) shows errors under 1.2 mm in Z-axis. After comparing results from Figure 8(b) with those from Figure 7(b), we concluded that our prototype with non-collinear LEDs reduced measurement errors using the PCMM as range meter. In Table 1 from Section 4.2.1, Liu et al. [3] report poor PCMM accuracy with collinear LEDs measuring one point and moving the hand tool in a different orientation to the camera. Based on this table, and supported by results from Figure 7(b), we concluded that collinear LEDs were not enough to get accuracies under millimeters. The decision to add more LEDs was consistent with Liu's, who changed from a collinear model in Liu et al. [3] to a non-collinear model in Liu et al. [5]. Finally, Figure 9 introduces the Z-axis errors of the PCMM

from Figure 8(a) before the LUT correction. Errors showed in Figure 8(b) confirmed that a simple LUT correction reduced the measurement error considerably.

5.4. Performance evaluation of PCMM under ASME B89.4.22-2004

A PCMM is similar to an AACMM, since both are manual and portable instruments and the measurement range is similar. Moreover, both instruments get coordinate system points in space referred to their own body; in the case of the AACMM, it is with respect to its base, whereas for the PCMM, it is referred to the camera. To assess the performance of our PCMM, we thus referred to ASME B89.4.22-2004 [24], who described a methodology for the performance evaluation of AACMM. The methodology includes three tests: the sphere test, the single point test and the volume test.

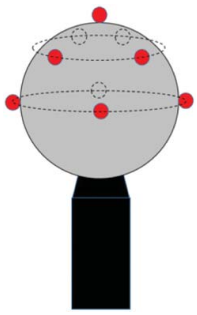

Figure 10. Sphere points to deal with sphere test.

Table 2. Effective diameter performance test of PCMM.

Measurement	1	2	3	Average	Standard deviation	Error
Sphere diameter (mm)	20.78	20.31	21.18	20.76	0.44	0.78

ASME B89.4.22-2004 [24] states that, to perform the sphere test, the sphere's diameter must be between 10 and 50 mm, and the sphere must be measured three times at the same location, and in approximately the middle of the PCMM range in our case. Also, the sphere diameter must be measured with nine points, fitting these points to a least square sphere. The distribution of points is as follows: four points equally distributed approximately on the equator, four points equally distributed at an approximate latitude of 45° and rotated at approximately 45° to those on the equator, and one point at the pole. Figure 10 shows the points location.

Table 2 shows the performance evaluation of our PCMM when it measures a sphere with nine points, fitted with a least square algorithm. The sphere's certificate reported a calibrated diameter of 19.98 mm. The error of Table 2 is equal to the average value minus the sphere's calibrated value.

Figure 11 shows the positions used to deal with the single point performance test (SPAT). As can be observed, we employed fewer positions than those specified by ASME B89.4.2.-2004 [24].

Table 3 shows the performance evaluation of the PCMM when it measures one point only:

where

$$L_i = \sqrt{(X_i - X_a)^2 + (Y_i - Y_a)^2 + (Z_i - Z_a)^2}; \quad (1)$$

$X_i, Y_i, Z_i =$ Measured coordinates

$X_a, Y_a, Z_a =$ Average coordinates

Table 3. Single point performance test results.

	X (mm)	Y (mm)	Z (mm)	Li	Li^2
1	−2.86	83.96	1066.10	0.32	0.10
2	−2.87	84.06	1065.90	0.15	0.02
3	−2.82	83.93	1066.40	0.62	0.39
4	−2.78	83.95	1065.50	0.29	0.08
5	−2.93	83.95	1065.00	0.78	0.61
Average	−2.85	83.97	1065.78		1.21
Li max	0.78				
2sSPAT	1.1				

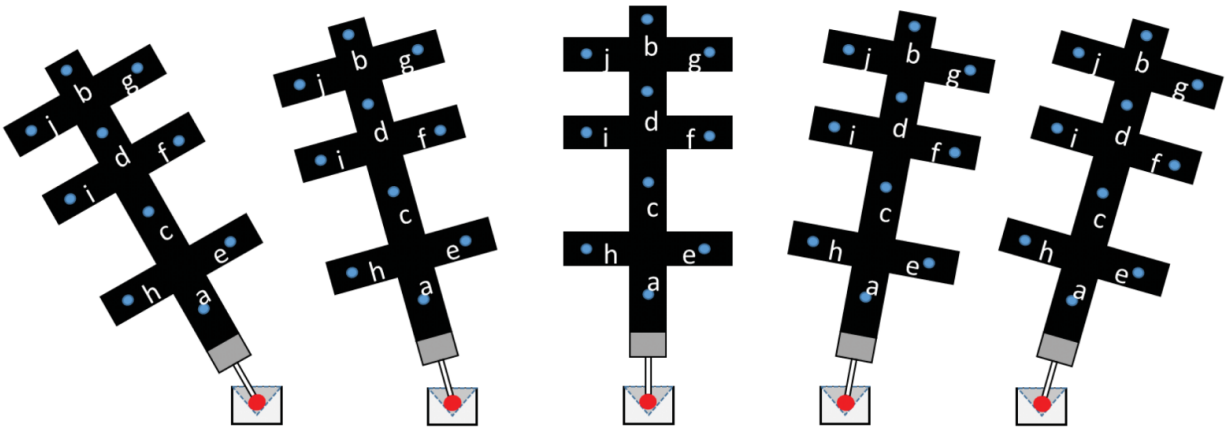

Figure 11. PCMM orientation to deal with single point performance test.

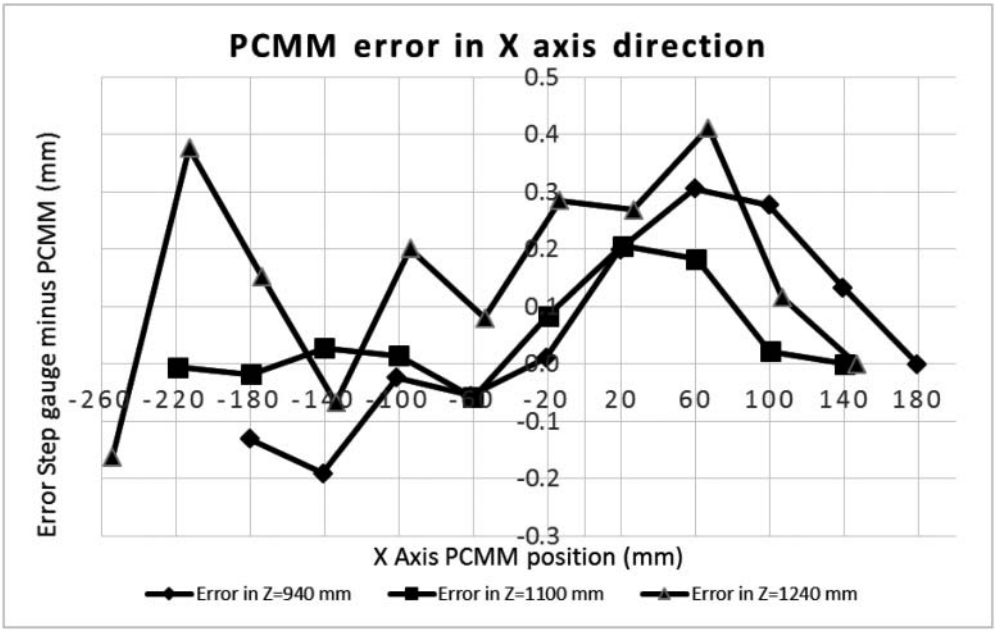

Figure 12. Errors of the PCMM measuring in *X*-axis direction at different *Z* positions.

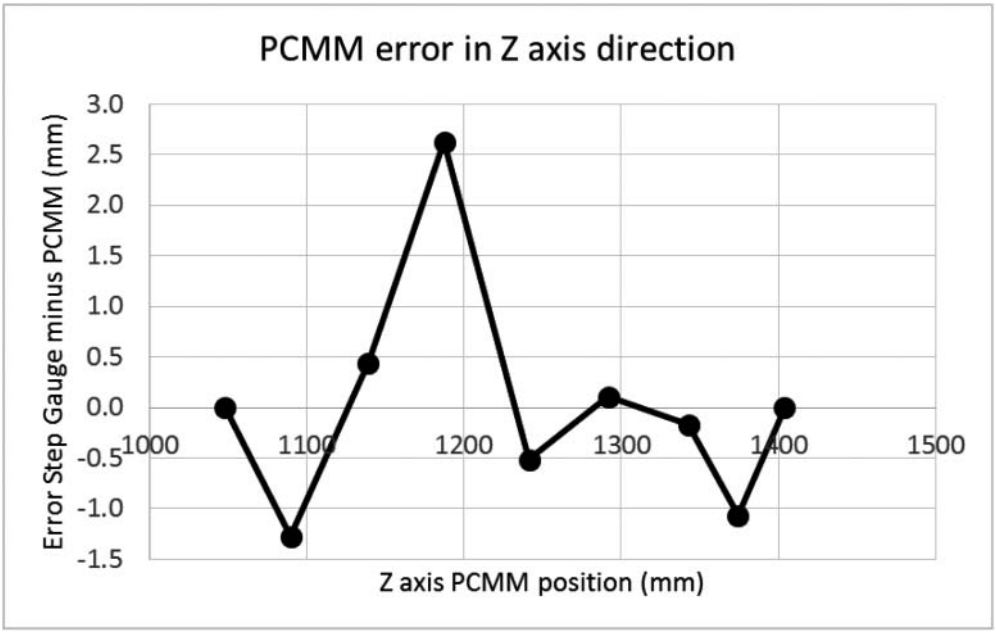

Figure 13. Errors of the PCMM measuring in *Z*-axis direction.

$$2\text{sSPAT} = 2\sqrt{\frac{\sum L_i^2}{(n-1)}} \tag{2}$$

2sSPAT = Single point articulation test.

In the volumetric performance test, ASME B89 .4.22-2004 [24] specifies at least 20 positions of a ball bar with a known distance between balls. However, because of the range of our PCMM, we conducted this test partially. In other words, we measured different distances between faces of a step gauge in *X* and *Z* directions, whereas *Y* direction was excluded due to the short PCMM's range in this direction. Based on the PCMM's coordinate system, depicted in past figures, the *X X*-axis had to be excluded, but an axis change transformation happened when we passed from the world to the camera system, thus causing the PCMM's *X X*-axis to be transformed into the *Y Y*-axis on the camera system.

Figure 12 shows the PCMM errors after measuring distances between faces of a step gauge of 400 mm long. The error reported in *X X*-axis of Figure 12 corresponds to the difference between the calibrated face-to-face distance values of the step gauge and the face-to-face distance measured with the PCMM. The errors represent the average of three measurements. Figure 12

shows a minimum influence of Z position on the reported errors in the X X-axis direction. Figures 12 and 13 present errors after LUT correction.

Figure 13 shows the PCMM errors in Z direction. This is the most critical direction of the PCMM, since it represented the distance between the camera and the hand tool. A hypothesis is that this direction and PCMM's POSE (especially hand tool's pitch and yaw movements) are the main source of errors.

6. Conclusions

In this paper, we proposed a PCMM. Note that to achieve proper geometrical shapes of circles, it is important to select appropriate LEDs. As regards the LED's position calibration with the OCMM and LED's tracking, we used centroids as references, but an ellipse contour may be preferred to avoid center location error (see [25]). Also, we selected a camera filter based on the wavelength emitted by the infrared LEDs. We believe that the circle's shape was influenced by the filter placed in front of the camera, which is why we selected an infrared band pass filter with a CWL and band width covering the LEDs' wavelength. The results obtained showed the emitted wavelength of a commercial infrared LED, which could be used as a reference value.

Any vision system used for dimensional measurements must perform camera calibration as the first step. In this sense, we thought that a printed pattern could be enough for the camera calibration, as long as a subsequent correction is performed. Moreover, according to Tang et al. [21], lens distortion is not well evaluated by Bouguet [18]. We will explore Tang's solution to see the influence of lens distortion on our PCMM measurements.

Also, in this work we propose an algorithm to track the LEDs attached to the hand tool. This algorithm can track and order the LEDs to identify them, no matter the hand tool's POSE. LEDs' order is an input parameter for the hand tool's POSE. POSE consumes little processing time not being iterative, but an accuracy test must be performed to know and correct the sources of error.

Our first prototype for the PCMM with collinear LEDs did not achieve the accuracy we were looking for (under millimeters). We believed this accuracy loss was due to orientation errors not evaluated correctly with collinear LEDs (see Table 1 of Liu et al. [3]). Therefore, we decided to modify the PCMM design, leading us to our initial goal. Also, according to Figures 8(b) and Figure 9, if the PCMM was used as a range meter, we could calculate a LUT correction and increase PCMM accuracy. We suggest using a CMM as a reference, but a step gauge or any other calibrated lengths could be used, although repeatability must be considered.

We evaluated the PCMM's performance under ASME B89.4.22-2004 standard, instead of developing a new, specific standard (see [1]). From the single point test, we concluded that a correct hand tool's POSE is crucial for small measurement errors (see [26–27]). As regards the PCMM design, it can be strengthened by replacing the aluminium part from the hand tool's body with a carbon-fiber-based one. Also, to reduce the hand tool's weight and dimensions, the Bluetooth module may be placed with another device. As a final remark for future work, we will test Lepetit's algorithm under controlled circumstances with dynamic but known POSES. Lepetit's algorithm is a key to preventing the use of iterative sequences, thereby reducing computational cost.

Disclosure statement

No potential conflict of interest was reported by the authors.

Funding

We thank Instituto Politécnico Nacional for its financial support through project [grant number SIP-20160023] and Centro Nacional de Metrología (CENAM) for the facilities granted through SIDEPRO program.

References

[1] Luhmann T. Close range photogrammetry for industrial applications. ISPRS J Photogramm Remote Sens. 2010;65(6):558–569.
[2] Hocken R, Pereira P. Coordinate measuring machines and systems. 2nd ed. Boca Raton (FL): CRC Press; 2011. Chapter 17, Non-Cartesian coordinate measuring systems; p. 495–497.
[3] Liu S, Huang F, Peng K. The modeling of portable 3D vision coordinate measuring system. SPIE Opt Des TestII. 2005;5638:835–842.
[4] Amdal K. Single camera system for close range industrial photogrammetry. In: Lawrence W, James R, editors. XVIIth ISPRS Congress; 1992 Aug 2–14; Washington DC. Washington (DC): ISPRS; 1992. Vol. 29. p. 6–10.
[5] Liu S, Zhang H, Dong Y, et al. Portable light pen 3D vision coordinate measuring system- probe tip center calibration. Meas Sci Rev. 2013;13(4):194–199.
[6] Li J, Zhao H, Fu Q, et al. New 3D high-accuracy optical coordinates measuring technique based on an infrared target and binocular stereo vision. Proc. Opt Meas Syst Ind Insp. 2009;7389:738925–1–738925–11.
[7] Xiao Z, Jin L, Yu D, et al. A cross-target-based accurate calibration method of binocular stereo systems with large-scale field-of-view. Meas J Int Meas Confederation. 2010;43(6):747–754.
[8] Lepetit V, Moreno-Noguer F, Pascal F. EPnP: an accurate O (n) solution to the PnP problem. Int J Comput Vis. 2009;81(2):155–166.
[9] Zheng Y, Kuang Y, Sugimoto S, et al. Revisiting the PnP problem: A fast, general and optimal solution. In: IEEE, editor. Proceedings of the IEEE International

Conference on Computer Vision; 2013 Dec 1–8. Sydney: IEEE. p. 2344–2351.
[10] Petersen T. A comparison of 2D-3D Pose estimation methods [master's thesis]. Lautrupvang: Aalborg University-Institute for Media Technology Computer Vision and Graphics; 2008.
[11] Alismail H, Browning B, Dias MB. Evaluating pose estimation methods for stereo visual odometry on robots. In: Christensen HI, Groen F, Petriu E, editors. Ebook: Intelligent Autonomous Systems 11 (IAS-11), University of Ottwa Canada; 2010 Aug 30–Sept 1; BG Amsterdam: IOS Press Ebooks; Aug 2010. p. 101–110.
[12] Kumar R, Hanson AR. Robust methods for estimating pose and a sensitivity analysis. CVGIP Image Underst. 1994;60(3):313–342.
[13] Lu CP, Hager GD, Mjolsness E. Fast and globally convergent pose estimation from video images. IEEE Trans Pattern Anal Mach Intell. 2000;22(6):610–622.
[14] Armstrong B, Verron T, Heppe L, et al. RGR-6D: low-cost, high-accuracy measurement of 6-DOF pose from a single image. Milwaukee (WI): Manuscript, University of Wisconsin; 2007.
[15] Rodehorst V, Heinrichs M, Hellwich O. Evaluation of relative pose estimation methods for multi-camera setups. Int Arch Photogramm Remote Sens. 2008;0 (3):135–140.
[16] Chang W, Chen C. Pose estimation for multiple camera systems. In: IEEE, editor. Proceedings of the 17th International Conference on Pattern Recognition 2004, ICPR 2004; 2004 Aug 26. Cambridge: IEEE. Vol. 3; 2004. p. 262–265.
[17] Zhang Z. A flexible new technique for camera calibration. IEEE Trans Pattern Anal Mach Intell. 2000;22 (11):1330–1334.
[18] Bouguet J-Y. Camera calibration toolbox for Matlab. Available from: http://www.vision.caltech.edu/bouguetj/calib_doc/
[19] Tsai R. A versatile camera calibration technique for high-accuracy 3D machine vision metrology using off-the-shelf TV cameras and lenses. IEEE J Robot Automat. 1987;3(4):323–344.
[20] Datta A, Kim J, Kanade T. Accurate camera calibration using iterative refinement of control points. In: IEEE, editor. 12th International Conference on Computer Vision Workshops, ICCV Workshops; 2009 Sept 27–Oct 4; Kyoto: IEEE. p. 1201–1208.
[21] Tang Z, von Gioi Grompone R, Monasse P, et al. High-precision camera distortion measurements with a calibration harp. J Opt Soc Amer A. 2012;29(10):2134–2143.
[22] Salvi J, Armangué X, Batlle J. A comparative review of camera calibrating methods with accuracy evaluation. Pattern Recognit. 2002;35(7):1617–1635.
[23] Zhu L, Luo H, Zhang X. Uncertainty and sensitivity analysis for camera calibration. Ind Robot Int J. 2009;36(3):238–243.
[24] The American Society of Mechanical Engineers. ASME B89.4.22-2004: methods for performance evaluation of articulated arm coordinate measuring machines (CMM). New York (NY): ASME; 2004.
[25] Jiandong Z, Liyan Z, Xiaoyu D. Accurate 3D target positioning in close range photogrammetry with implicit image correction. Chin J Aeronaut. 2009;22(6):649–657.
[26] Luhmann T. Precision potential of photogrammetric 6DOF pose estimation with a single camera. ISPRS J Photogramm Remote Sens. 2009;64(3):275–284.
[27] Luhmann T, Fraser C, Maas HG. Sensor modelling and camera calibration for close-range photogrammetry. ISPRS J Photogramm Remote Sens. 2016;115:37–46.